Quantitative Assessment of Morphological Changes in Lipid Droplets and Lipid-Mito Interactions with Aging in Brown Adipose

Authors: Amber Crabtree[1,2], Kit Neikirk[1*], Aaron Whiteside[1*], Jessica McKenzie[1], Zer Vue[1], Larry Vang[1], Trinity Celeste Owens[1], Ashton Oliver[1], Faben Zeleke[1], Heather K. Beasley[1], Edgar Garza Lopez[3], Estevão Scudese[1], Alice Koh[1], Suzanne Navarro[1], Jacob Lam[3], Ben Kirk[3], Margaret Mungai[3], Mariya Sweetwyne[4], Ho-Jin Koh[5], Elma Zaganjor[1], Steven M. Damo[6], Jennifer A. Gaddy[7], Clintoria Williams[8], Melanie R. McReynolds[9], Andrea G. Marshall[1#], Antentor Hinton, Jr.[1#]

[1] Department of Molecular Physiology and Biophysics, Vanderbilt University, Nashville, TN, 37232, USA.

[2] The Frist Center for Autism and Innovation, Vanderbilt University, Nashville, TN, 37212, USA.

[3] Department of Internal Medicine, University of Iowa, Iowa City, IA, 52242, USA

[4] Department of Laboratory Medicine and Pathology, University of Washington, Seattle, WA, 98195, USA.

[5] Department of Biological Sciences, Tennessee State University, Nashville, TN 37209, USA

[6] Department of Life and Physical Sciences, Fisk University, Nashville, TN, 37208, USA.

[7] Division of Infectious Diseases, Vanderbilt University School of Medicine, Nashville, TN, 37232, USA; Tennessee Valley Healthcare Systems, U.S. Department of Veterans Affairs, Nashville, TN, 37212, USA.

[8] Department of Neuroscience, Cell Biology and Physiology, Wright State University, Dayton, OH 45435 USA.

[9] Department of Biochemistry and Molecular Biology, Pennsylvania State University, University Park, PA; Huck Institutes of the Life Sciences, Pennsylvania State University, University Park, PA, USA.

* indicates co-second authorship
# indicates co-senior authorship

Correspondence:
antentor.o.hinton.jr@vanderbilt.edu

ABSTRACT

The physical characteristics of brown adipose tissue (BAT) is defined by the presence of multilocular adipocytes and a high abundance of iron-containing mitochondria which give it its characteristic color. Normal mitochondrial function is regulated by organelle-to-organelle contacts, among other things. The contact sites of mitochondria-lipid droplet (LD) interactions have been implicated in various physiological roles such as the synthesis and metabolism of lipids. Importantly, past data has found that across the aging process, in addition to mitochondrial dysfunction, there are changes in mitochondrial structure as well as proteins that modulate contact sites. Here, we sought to define age-related changes in LD morphology and mito-lipid interactions in BAT. To accomplish this, we examined the three-dimensional morphology of mitochondria and LDs in young (3-month) and aged (2-year) murine BAT tissue via serial block face-scanning electron microscopy and the Amira program for segmentation, analysis, and quantification. Upon analysis, we found reductions in LD volume, area, and perimeter in 2-year-aged BAT murine samples compared to 3-month murine samples. Additionally, we observed changes in LD appearance and type in 2-year-aged BAT murine samples compared to 3-month murine samples. Notably, we found differences in mitochondrial interactions with lipids, which could implicate that, with age, contacts may be important for energetics. Upon further investigation, we also found changes in mitochondrial structure for mitochondria interacting with lipids. Overall, these data define the nature of the LD morphology and organelle-organelle contacts during aging and provide insight into lipid contact site changes that could have implications on mitochondrial functionality, metabolism, and bioactivity in aged BAT.

Keywords: BAT; Mitochondria; LDs; Mito-Lipid; Lipids

INTRODUCTION

Although mitochondria have numerous indispensable functions, including the maintenance of calcium homeostasis, their most notorious role is for being the primary energy producers of the cell (1). Within mitochondrial networks, the function of each mitochondrion is believed to be both tissue and cell-type dependent (2,3). As mitochondrial function is tightly associated with mitochondrial morphology, mitochondrial ultrastructure changes in accordance with the energetic and functional demands of the cell (2,4). Consistent with this, functional and subsequently, morphological, heterogeneity is observed in various tissue and cell types. Mitochondrial heterogeneity is also observed within each cell and is believed, in part, to be dependent on subcellular localization and the dynamic nature of mitochondria (2,3).

Mitochondrial dynamics consist of coordinated cycles of fusion and fission which provide a means for content mixing, quality control, and the maintenance of healthy mitochondrial networks (5). In brown adipose tissue (BAT), the reorganization of the mitochondrial ultrastructure works cooperatively with the release of free fatty acids to promote heat production via uncoupled respiration (6,7). Immediately following cold exposure or adrenergic stimulation, mitochondrial fission is promoted, a process shown to be essential for

BAT thermogenesis (7,8). Moreover, recent studies have highlighted the significance of mitochondrial architecture in maintaining thermogenic capacity and energy homeostasis in BAT (9–11). During the aging process, a functional decline in BAT is observed and is associated with the onset of metabolic disorders, including type II diabetes.

Recently, we showed that a loss of the inner mitochondrial folds, known as cristae, occurs while the mitochondrial volume and matrix both increase with aging in murine BAT (12). Although the high abundance of mitochondria is probably the most noted characteristic of thermogenic adipose tissue, it is not the only defining characteristic. Multilocular LDs, as opposed to the unilocular LDs observed white adipose tissue are also a defining feature of thermogenic adipose tissue (13). Studies have shown that the composition and distribution of lipids in BAT can alter mitochondrial function and efficiency (14–16), with potential implications for age-related decline in thermogenic capacity. Additionally, across aging, BAT has been illustrated to have an accumulation of phospholipids, sphingolipids, and dolichols (17) which points toward increased LD formation that may be counteracted by mitochondria-LD-mediated lipolysis (18–20).

Mitochondria are known to make contact and associate with other organelles, including other mitochondria, allowing for highly regulated fine-tuning of vital processes such as calcium signaling, lipid synthesis, apoptosis, and the formation of autophagosomes (14,20–22). In various oxidative tissues, mitochondria and LDs show extensive interaction networks. In BAT, mitochondria-LD interactions increase following cold stimulation, presumably to facilitate fatty acid consumption for thermogenesis (13,14,23,24). These interactions are categorized into either dynamic or stable subgroups according to their interaction strength (23,25,26). Dynamic interactions are those that can be disrupted using high speed centrifugation which include peridroplet mitochondria, whereas stable interactions remain undisrupted using high speed centrifugation and are also known as LD-anchored mitochondria (13,14). Although our understanding of mitochondria-LD interactions is evolving, the exact changes that occur with these organelle contacts across aging remains incompletely understood.

To better examine how the aging process affects LDs and their associations with mitochondria in murine BAT, we utilized serial block-face scanning electron microscopy (SBF-SEM) and 3D reconstruction to quantitatively study these organelle interactions with relatively high spatial resolution (27–29). To ensure the highest accuracy, we employed manual mitochondria and LD contour tracing using previously validated techniques (30). We hypothesized that changes in mitochondria-lipid interactions and lipid morphology dynamics would be observable across aging in a male murine BAT model. As the first to study 3D organelle-organelle contacts in adipose tissue across aging, we characterized structural changes that may yield valuable insights into the age-related decline in BAT thermogenic capacity and mitochondrial function.

METHODS

Animal Housing and Care

C57BL/6J male mice were housed at 22□ C with ad libitum food and water intake and maintained with alternating 12-hr dark/12-hr light cycles. Mice were cared for as previously described by Lam et al. (2021) (31). All animal protocols were approved by the University of Iowa Animal Care and Use Committee.

SBF-SEM Sample Preparation

Interscapular BAT depots were excised from 3-month and 2-year aged mice following euthanasia and fixed in 2% glutaraldehyde in 0.1M cacodylate buffer. A heavy metal protocol was used for processing. Samples were washed with deionized H_2O (diH_2O) then immersed in 3% potassium ferrocyanide, followed by 2% osmium tetroxide, at 4□ C for 1-hour each. Samples were immersed in filtered 0.1% thiocarbohydrazide for 20 minutes following diH_2O wash. Samples were washed again in diH_2O, then immersed in 2% osmium tetroxide for 30 minutes. Samples were incubated overnight in 1% uranyl acetate at 4□ C prior to incubation in 0.6% lead aspartate for 30 minutes at 60□ C. An ethanol graded series dehydration was then performed prior to samples being infiltrated with epoxy Taab 812 hard resin. Samples were then immersed in fresh resin and polymerized at 60□ C for 36-48 hours. Transmission electron microscopy (TEM) was utilized to identify regions of interest for each of the resultant resin blocks. Samples were trimmed and glued to an SEM stub prior to being placed into a FEI/Thermo Scientific Volumescope 2 SEM. 300-400 serial sections of 0.09 μm thickness were obtained and collected per sample block. The micrograph blocks were then aligned, manually segmented, and 3D-reconstructed using Thermo Scientific Amira Software (Waltham, MA, USA) per previously described (21,30,32).

Mitochondrial and LD Ultrastructure Calculations and Measurements

Label analyses were performed following manual segmentation of LDs and lipid-associated mitochondria in the regions of interest (ROIs). Each segmented structure was then subject to label analysis using Amira (1). Blinded-3D structural reconstruction from at least three independent experiments was performed to obtain the SBF-SEM murine BAT data. Sequential orthoslices were manually segmented to obtain 300-400 slices for each 3D reconstruction. 50-200 serial sections were then chosen for each 3D reconstruction at approximately equal z-direction intervals. Serial sections were then stacked, aligned, and visualized using Amira software. All videos and volumetric structure quantifications were generated using Amira software. Measurement algorithms that were not already in the system were manually entered. All mitochondria associated with LDs were manually segmented (Figure 2). A total of ~800 (3-months) and ~1100 (2-years) mitochondria associated with LDs were collected for quantification from two mice.

Structure Quantifications and Statistic Analyses

Statistical analyses of all label analysis data and manual measurements were analyzed using a student's t-test, or the non-parametric equivalent where applicable, in GraphPad Prism (San Diego, California, USA). Individual data points are depicted by dots and all data are considered biological replicates unless otherwise specified. All outliers were used for statistical analyses but may not be displayed for presentation purposes. Graphs are depicted as means with standard

error mean (SEM) indicated as black bars. Statistical significance was defined as $p < 0.05$ (*), $p < 0.01$ (**), $p < 0.001$ (***), and $p < 0.0001$ (****).

RESULTS

Murine BAT Shows Smaller LDs Across Aging with No Changes in Total Cellular Lipid Volume

Intrascupular BAT tissue was extracted from mice aged 3-months-old (representing "young adults") and 2-years-old (representing "geriatric"). To consider the 3D dynamics of both LDs and mitochondria-lipid interactions across aging, SBF-SEM was utilized as it provides a high spatial resolution (10 µm for the x- and y-planes and 50 µm for the z-plane) while also allowing for large volumes to be surveyed (27). 3D reconstructions were performed using previously described methods (21). For each age group (n=3) approximately 100 LDs were surveyed, for a total of 600 LDs between separate regions of interest in young and old mice (Figure 1A). 3D reconstruction was performed by the manual contour tracing of 50 images of 50-µm block ortho slices (Figure 1B) across standard transverse intervals (Figure 1C) to enable the reconstruction of pseudocolored LDs (Figure 1D).

Using this workflow of SBF-SEM-based 3D reconstruction, orthoslices (Figure 2A) were overlaid for 3D reconstruction (Figure 2A') of LDs. Based on these representative orthoslices, detailed 3D reconstruction of LDs was rendered (Figure 2A'') in both 3-month and 2-year (Figure 2B-B'') male murine samples. Cohort age groups were selected as 3 months, which is considered life phase equivalent to 20 years of age in humans, and 2-years, which is considered approximately 69 years of age in humans (33).

Notably, in young samples, we noticed that many individual LDs were too large to fit inside the region of interest, despite the relatively large range of SBF-SEM (10 µm by 10 µm) (27). Although this means that the values for 3-month samples are less reliable, it also demonstrates that there are significant reductions in LD volumes across aging. We also found that with aging, murine BAT lipid droplets significantly decrease in 3D area (Figure 2C) and volume (Figure 2D). Furthermore, it is unlikely this data arrangement occurred due to some lipids falling outside of the range, as the total cellular volume with lipids showed a marked decrease (Figure 2E). Alongside this, we noted that perimeter had a significant decrease (Figure 2F). When comparing the LDs quantifications from each mouse, they exhibited minimal inter-group heterogeneity but consistent intra-group variability with slightly decreased heterogeneity in aged samples (SFigure 1). Together, this indicates an age-dependent loss in lipid droplet total size and average size.

Past studies have demonstrated a way to organize mitochondria in a karyotype-like arrangement on the basis of volume (12,34–36). Here, we adapt this method to form a "lipid-otype" organization which allows for the structure and complexity of LDs of various relatively similar volumes to be compared across the age conditions (Figure 3A). This shows a relatively even distribution of lipid sizes with slightly increased roundness in aged samples. To verify these changes in the general roundness of LDs across BAT aging, we calculated lipid sphericity as $\frac{\pi^{\frac{1}{3}}(6*Volume)^{\frac{2}{3}}}{Surface\ Area}$). We found that lipid droplet sphericity increased with aging in murine BAT

(Figure 3B). Consistent with this, we also found that the complexity, which is inversely related to sphericity, of lipid droplet 3D structures decreased with age (Figure 3C). Together, this indicates an age-dependent decrease in both age of lipid droplets, while sphericity also altered indicating changes in morphology. To better understand if the wider cellular environment was concomitantly changing with these morphological changes, we decided to look at possible changes in mitochondrial interactions with lipids across aging.

BAT 3D Reconstruction shows Altered Mito-Lipid Interactions Across Aging

Using the same BAT ROIs that were used for lipid droplet quantifications, we sought to quantify the mitochondria-lipid interactions in both age groups (Figure 4A-E). Using a similar workflow, male murine mice have intrascapular brown adipose tissue extracted (Figure 4A) and subject to for SBF-SEM imaging (Figure 4B). Here, lipid associated mitochondria were identified (Figure 4C), and manual contour tracing was done to calculate the contacts between them and the lipid droplets (Figure 4D). In many cases, we notably found that mitochondria could interact with up to 4 different lipid droplets simultaneously, owing in part to the large volume of lipid droplets in BAT (Figure 4E). Given the many interactions, we randomly selected two mice (n=2) and surveyed interactions from these samples for approximately 800 total interactions in 3 month samples and 1100 interactions in 2 year samples.

Using this workflow, starting from 3-month and 2-year orthoslice (Figure 5A-B), we reconstructed lipid droplets (Figure 5A’-B’), mitochondria (Figure 5A’’-B’’), and subsequent isolated contacts which these two organelles form (Figure 5A’’’-B’’’). We found a slight but statistically insignificant change in the percent of total mitochondria present interacting with lipid droplets in 2-year samples (Figure 5C). Interestingly, however, when disaggregating on the basis of the number of contacts formed, we observed that single interactions decreased, while the proportion of mitochondria interacting with 2, 3, or 4 lipids remained consistent in aged samples (Figure 5D-E). Together, these results indicate that with age lipid droplets increasingly interact with mitochondria with a propensity for multiple interaction sites, although not with a significant difference. Next, we wanted to see if there were any changes in the mitochondrial and lipid surfaces interacting in these aged samples.

When comparing the percent of mitochondrial perimeter and surface area in contact with LDs, we found significant decreases across aging (Figure 5 F & H). In contrast, the percentage of mitochondrial perimeter and surface area in contact with mitochondria increased significantly with aging, likely due to the smaller size and more abundant presence of lipid droplets in the 2-year aged group (Figure 5 G&I). This indicates that with age, a lower percentage of the total surface of mitochondria are dedicated to mito-lipid interactions while the inverse is true for lipid droplets. Given we have previously reported mitochondria get larger with aging in BAT (12), and lipid droplets get smaller, part of these results may arise given this inverse change in sizes. Given lipid droplets were interacting with many mitochondria often, we wanted to understand if the total percentage of surface area of a lipid droplet engaged in interactions changed. We showed there was a similar increased, from around 10% to 15%, indicating that both individual contacts (Figure 5 G, I) and cumulative contacts (Figure 5J) increased relative to lipid droplet surface area.

Finally, we looked at age-related changes that occur with the contact sites themselves. We found that the average volume and surface area of each mitochondria-LD contact showed significant decreases across aging (Figure 5 K&L). This may indicate that the contact sites are decreasing in surface area, with a potential tightening of these contacts resulted in reduced volume. Notably, in these studies, we showed large heterogeneity between the three ROIs surveyed, indicating variance both intra- and inter-samples. However, contact sites can both be measured by the tightness of their junctions as well as the amount of organelle in contact with each other.

3D Reconstruction Shows Mito-Lipid Interactions Do Not Cause Alterations in Mitochondrial Morphology

From there, we questioned if altered morphology would be present across mitochondrial subpopulations when comparing cytosolic mitochondria to those interacting with LDs. Significant contact was defined as mitochondria with >20% of the mitochondria perimeter interacting with LDs (23). It has been reported that subpopulations of mitochondria are functionally distinct from each other (14). While we previously considered all mitochondrial volume in aged BAT samples (12), here, we sought to classify the phenotypes of the mitochondrial subpopulations. Using the same 2 ROIs, orthoslices were viewed in 3 month (Figure 6A) and 2-year (Figure 6B) murine BAT tissue, and manual contour tracing allowed for 3D reconstructions. Specifically, two distinct populations of mitochondria, peri-droplet and cytoplasmic, were selected for and, once 3D reconstructed they can be overlaid on orthoslices (Figure 6A’-6B’) or viewed isolated (Figure 6A’’-6B’’). These interactions were verified from multiple viewpoints to validate their analysis (Figure 6C-D). We found that with age, as expected from our previous results (12), mitochondrial length and width both increased (Figure 6E-F). Yet, there were generally non-significant differences in mitochondrial width and length. Notably, we did see that while for non-interacting mitochondrial had no age-related increase in width, lipid-associated mitochondria did have a significant difference, indicating that age-related changes may attenuate alterations due to proximity to LDs. Together, these results indicate that both the size of mitochondria-lipid droplet interactions changed on the basis of aging, while subpopulations of mitochondria may not always dynamically change in response to these alterations in contact sites.

DISCUSSION

In the present study, 3D quantification of lipid droplets and the mitochondria that interact with them showed distinct age-related differences in a male murine BAT. We found age-dependent losses in size, alongside altered distribution and shape of LDs in BAT. These findings are contradictory to other reports of increased cytoplasmic LD size in BAT with aging in both male (37) and female (38) mouse models. However, it should be noted different sub-populations of brown adipocytes exist, with low-thermogenic activity populations exhibiting larger LDs, while high-thermogenic brown adipocytes have smaller LDs (39). Additionally, numerous factors could contribute to the variance seen including, but not limited to, differences in chow diet composition, microbiome, and housing conditions. Moreover, the previous studies mentioned did not quantify lipid droplet size differences using 3D methods, like those utilized in

the current study which is also likely a contributing factor to the differences seen in the results reported. Critically, our results point towards mitochondria-LD interactions which decrease LD volume. However, further studies are needed before any conclusions can be drawn.

Interestingly, we also noticed tri-organelle interactions with mitochondria-mitochondria interactions occurring between mitochondria interacting with LDs and those not interacting (Figure 5). It is possible this is a tri-organelle contact site, as has previously been reported through ER, mitochondria, and peroxisomes (40). However, the functional relevance of mitochondria-mitochondria contact sites has not been well established. Equally possible, these decreased mitochondrial separation distances may be indicative of post- or pre-mitochondrial dynamic events (41). Similarly, we also noticed many mitochondria interacted with more than one lipid droplets; it is possible that there are different bioenergetics on the basis of the quantity of lipid droplets interacted with. Notably, we did not consider how mitochondrial quantifications changed on the basis of the number of interactions. Thus, it is possible that there are significant differences when considering mitochondrial quantification on the basis of interaction count, which future studies may examine.

Equally, as lipid-associated mitochondria change in architecture compared to cytoplasmic mitochondria, it is possible peridroplet mitochondria support the growth of lipid droplets for future triglyceride lipolysis through alterations in bioenergetics. Changes in mitochondrial-lipid interactions, may affect the efficiency of energy production and thermogenesis, that may lead to impaired lipid utilization and compromised mitochondrial function in aged BAT (14,23,42). There is a unique balance in BAT, where LD-mitochondrial contact sites both drive fatty acid oxidation and reduce LDs size (13,14,20), while peridroplet mitochondria have distinct protein levels, engage primarily in pyruvate-derived energy, and expand LDs through the synthesis of TAGs (23,43). Critically, our results point towards mitochondria-LD interactions which decrease LD volume. Here, while biochemically we could not differentiate between these subpopulations, our results indicate that we primarily towards the “kiss and run” models, indicating that these structural changes may result in increased fatty acid oxidation (13,14,20). This differs from the literature (23) and suggests that the relationship between LDs and mitochondrial interactions, as well as potential roles in fatty acid oxidation, must be further explored.

Past studies have shown that across aging, there is a change in the regulation of metabolites related to energy metabolism, nucleotide metabolism, and vitamin metabolism (44). Notably, *de novo* purine nucleotide synthesis is downregulated across aging (44). It is possible that the morphology we observe here may contribute to this, as mitochondria are well understood to be involved in de novo purine nucleotide synthesis through various intermediates such as amidophosphoribosyl transferase (45). Energy metabolism is also increased across the aging process, while hexokinase 1, a rate-limiting catalysis in glycolysis, is upregulated during aging (44). This suggests that across aging, mitochondria oxidative phosphorylation may be impaired while LD-mitochondrial may serve as an alternative mechanism for fatty acid oxidation as an alternative energy source. Yet, different fatty acids are known to have differential effects on LD-mitochondrial interactions; for example, while palmitic acid overload fuels fatty acid oxidation, oleic acid presented a different phenotype of increased LD-mitochondrial contact sites yet also

increased lipid content, suggesting metabolically inactive mitochondria (46). It remains unclear if these age-related metabolic changes are distinct across PDMs and CM subpopulations. To better explore these age-related alterations, future studies should further examine both age-related changes in mitochondria-bound LD composition (23,43) and protein levels known to link LDs and mitochondria such as PLN1, PLN5, and MFN2.

There are several important limitations of our study that should be noted. First, studies show that there are distinct populations of brown adipocytes with either high or low-thermogenic activity. Aside from different expression levels of *Ucp1*, these adipocytes also differ in lipid droplet size and mitochondrial content (39). Our study did not account for this heterogeneity in the BAT population, which may contribute to some of the variation observed in organelle morphology. Future studies may consider 3D tissue profiling to see if contact site structure varies across populations of adipocytes or *Ucp1* expression (39). Additionally, while LDs and mitochondria form dynamic contact sites, they can also form tight-bound interactions which cannot be separated using ultracentrifugation and have altered physiological functions centered around LD expansion and oxidative functions (23,24,43,47). However, in contrast to mitochondria-endoplasmic reticulum contact sites, which have clearly defined thickness (22), the distance between dynamic and tight/stable LD-mitochondria interactions remains poorly studied, limiting the ability for differentiation and comparison.

It is also important to note that while the murine model allows for the study of BAT across aging, it also can differ from human BAT. Interscapular BAT, as studied here, often does not exist in humans past early childhood, while the thermogenic roles of BAT are more fundamental to small rodents than humans (48). This makes the roles of human BAT less clear, especially in the context of the age-dependent loss of BAT observed in humans (48). Additionally, only male mice were used in this study. This is important to note as sexual dimorphism also has relevance in physiological function as BAT from women can display altered expression of certain proteins such as UCP1 (49,50). Furthermore, sex-dependent differences can manifest as independent aging-dependent responses, such as in puberty where BAT is more plentiful and active in boys (51). While BAT has commonalities across sexes, these model and sex-dependent differences should be considered in the interpretation of results, and future studies should aim to further elucidate the 3D structure of human mitochondrial organelle contacts in BAT.

Overall, this study defines the age-related changes in LD 3D morphology and mito-lipid interactions, which could collectively contribute to the decline in thermogenic capacity and mitochondrial function in aged BAT. Understanding these changes may provide valuable insights into age-associated metabolic disorders and inform potential therapeutic strategies targeting these dysfunctions. Our studies demonstrate the importance of also considering organelle contact sites as opposed to mitochondrial morphology alone in consideration of structural changes that may be occurring in response to disease or aged states.

Declaration of interests

The authors have no Conflicts of Interest to declare.

Contributions:

A.C. performed the experimental procedures, data analysis, interpretation of results, and writing of the manuscript.

K.N., A.W., and J.M. contributed equally to this work. They performed the experimental procedures, data analysis, interpretation of results, and writing of the manuscript.

Z.V., L.V., T.C.O., A.O., F.Z., H.K.B., E.G.L., E.S., A.K., S.N., J.L., B.K., and M.M. were involved in data collection, analysis, and interpretation.

S.M.D., J.A.G., C.W., M.R.M., M.S., H.J.K., and E.Z. provided critical feedback, contributed to the writing and revision of the manuscript, and assisted in various aspects of the research.

A.G.M and A.H. Jr. conceptualized the study, provided overall guidance, supervised the research, and revised the manuscript.

Acknowledgments

Funding by the UNCF/Bristol-Myers Squibb E.E. Just Faculty Fund, BWF Career Awards at the Scientific Interface Award, BWF Ad-hoc Award, NIH Small Research Pilot Subaward to 5R25HL106365-12 from the National Institutes of Health PRIDE Program, DK020593, Vanderbilt Diabetes and Research Training Center for DRTC Alzheimer's Disease Pilot & Feasibility Program. T-32, number DK007563 entitled Multidisciplinary Training in Molecular Endocrinology to A.C. NSF NRT grant 19-22697 and NSF BPE grant 22-17621 (K. Stassun, PI) to A.C.; T-32, number DK007563 entitled Multidisciplinary Training in Molecular Endocrinology to Z.V. CZI Science Diversity Leadership grant number 2022- 253529 from the Chan Zuckerberg Initiative DAF, an advised fund of Silicon Valley Community Foundation (to AHJ). NSF EES2112556, NSF EES1817282, NSF MCB1955975, and CZI Science Diversity Leadership grant number 2022-253614 from the Chan Zuckerberg Initiative DAF, an advised fund of Silicon Valley Community Foundation (to S.D.). NSF grant MCB #2011577I to S.A.M. NIH K01AG062757 to M.T.S. I01 BX005352 from the Dept. of Veterans Affairs Office of Research to J.A.G.

References

Automatic citation updates are disabled. To see the bibliography, click Refresh in the Zotero tab.

Figure Legends:

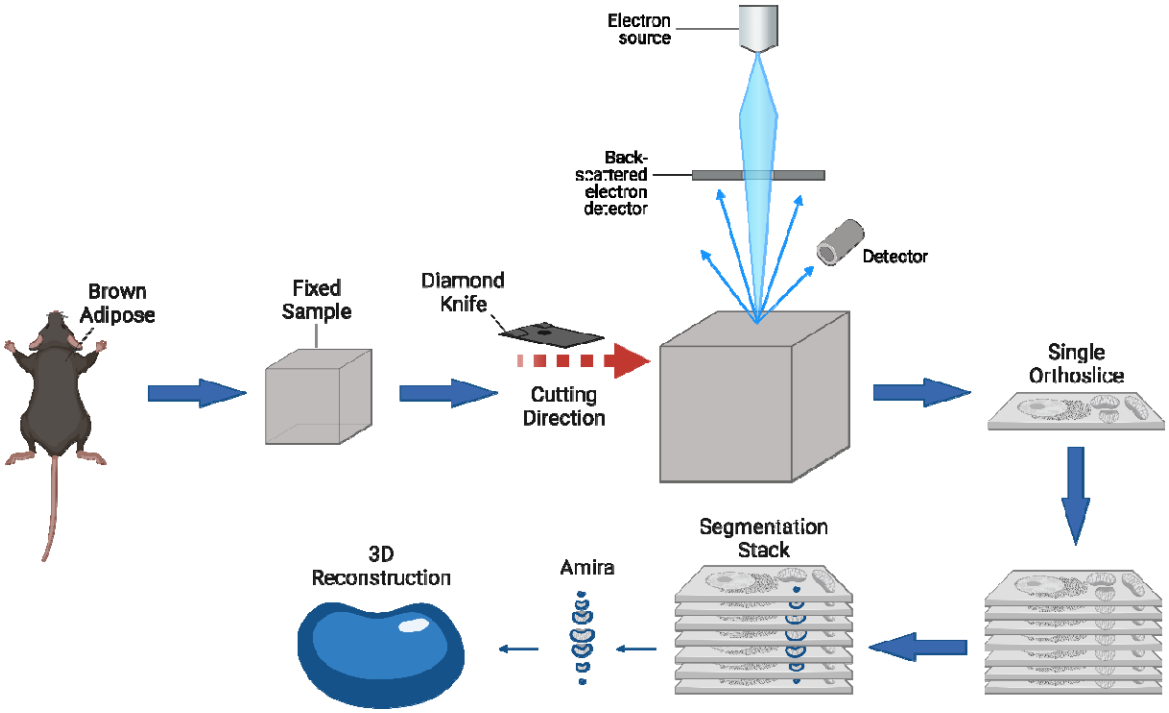

Graphical Abstract: Workflow highlighting the process of murine interscapular BAT extraction, processing and imaging serial block facing-scanning electron microscopy, and using Amira software for 3D reconstruction of LDs and mitochondrial lipid contact sites to elucidate their structure across aging.

Figure 1: Detailed 3D reconstruction workflow for lipid droplets using serial block face-scanning electron microscopy (SBF-SEM). (A) Interscapular brown adipose tissue (BAT) excised from male C57BL/6J mice. (B) High-resolution 10 µm by 10 µm orthoslices were generated by imaging, aligning, and stacking consecutive ultrathin sections of the sample. (C) SBF-SEM images had lipid droplets manually traced to create representative orthoslices, which provided valuable information on the internal structure of the mitochondria. (D) A detailed 3D reconstruction of lipid droplets was produced based on this workflow, allowing for in-depth analysis of lipid droplet size and complexity.

Figure 2: Analysis of mitochondrial morphology changes during the aging process. (A) 3-month-old and (B) 2-year old murine BAT showing: a representative orthoslice; (A'-B') 3D reconstruction of lipid droplet overlaid on the orthoslice; (A''-B'') Isolated 3D reconstruction with orthoslice removed, highlighting the individual mitochondrial structure. (C) Quantitative comparison of 3D lipid droplet area, (D) volume per lipid droplet, (E) cumulative lipid droplet volume, and (F) perimeter between 3-month and 2-year samples to assess morphological differences, revealing age-related changes in size of lipid droplets. Unpaired t-test was used to evaluate changes, with a variable sample number (n approximately 75), with each individual mice's average represented by black dots. $p < 0.0001$ indicated by ****.

Figure 3: Analysis of age-related changes in lipid complexity. (A) Lipid-otyping for lipid droplet morphology in 3-month and 2-year murine BAT samples based on volume, providing insights into the age-related alterations in structural complexity. These changes in complexity quantitatively comparison of (B) 3D sphericity and (C) complexity index. Unpaired t-test was used to evaluate changes, with a variable sample number (n approximately 75), with each individual mice's average represented by black dots. $p < 0.001$ and $p < 0.0001$ are indicated by *** and ****, respectively.

Figure 4: Workflow of serial block face-scanning electron microscopy-based 3D reconstruction for mitochondria-lipid interactions. (A) Brown adipose tissue was excised from 3-month and 2-year aged male C57BL/6J mice. (B) 10 µm by 10 µm orthoslices were overlaid for 3D reconstruction. (C) Lipid-associated mitochondria were identified and (D) manually contour traced, as shown in representative orthoslices from SBF-SEM slices. (E) Diagram of representative images of 1, 2, 3, and 4-lipid droplet interacting mitochondria.

Figure 5: Changes in mitochondria-lipid droplet morphology and frequency across aging. (A-B) Murine BAT representative orthoslice, (A'-B') 3D reconstruction of lipid droplet (yellow) overlaid on orthoslice, (A''-B'') 3D reconstruction of lipid droplet (yellow) and mitochondria (blue) overlaid on orthoslice, and (A'''-B''') 3D reconstruction mitochondria and lipid droplets in 3-month (A-A''') and 2-year samples (B-B'''). (C-I) Quantification of the lipid droplet-mitochondria contact sites. (C) Comparisons of proportion of lipid associated mitochondria to cytoplasmic mitochondria. (D) Mitochondrial distribution on the basis of number of lipid interactions formed by count and (E) relative percent. (F) percent contact site perimeter coverage relative to total mitochondrial perimeter, (G) percent contact site perimeter coverage relative to total lipid perimeter, (H) percent contact site surface area coverage relative to total mitochondrial surface area, (I) percent contact site surface area coverage relative to total lipid droplet surface area, (J) percent total contact site surface area coverage relative to total lipid droplet surface area. Average (K) volume of each contact, and (L) surface area of each contact were further elucidated. Unpaired t-test was used to evaluate changes, with a variable sample number (n

approximately 400), with each individual mouse's average represented by black dots. $p < 0.05$, $p < 0.01$, $p < 0.001$, and $p < 0.0001$ are indicated by *, **, ***, and ****, respectively.

Figure 6: Lipid-Associated Mitochondria Show Distinct Subpopulation Changes in Mitochondrial Architecture. (A) 3-month murine BAT mitochondria viewed from orthoslice, allowing for fine details to be elucidated; (A') reconstruction of mitochondria and mitochondria associated with lipid droplets (A'') isolated 3D reconstruction of isolated mitochondria (pink) and lipid-associated mitochondria (blue). (B) 2-year murine BAT mitochondria viewed from orthoslice, allowing for fine details to be elucidated; (B') reconstruction of mitochondria and mitochondria associated with lipid droplets, (B'') isolated 3D reconstruction of isolated mitochondria (pink) and lipid-associated mitochondria (blue). (C) Mitochondria associations with lipid droplets viewed from the xy-plane and (D) yz-plane. (E) Comparisons of mitochondrial 3D length and (F) width across aging and on the basis of age and if interacting with lipid droplets. Kruskal–Wallis one-way analysis of variance with post-hoc pairwise comparison test comparing each mean of groups, was used to evaluate changes, with a variable sample number (n approximately 33), with each individual mouse's average represented by black dots. $p < 0.05$, $p < 0.01$, $p < 0.001$, and $p < 0.0001$ are indicated by *, **, ***, and ****, respectively.

Supplemental:

Supplemental Figure 1: Display of raw lipid droplet quantifications. Each bar represents one of the three regions of interest surveyed at respective age points while dots represent individual lipid droplets (n is approximately 75, but varies). Values are displayed for lipid (A) volume, (B) area, (C) perimeter, (D) complexity index, and (E) sphericity.

Video 1: Depiction of z-directional ortho slices used to reconstruct lipid droplets in 3-month murine brown adipose tissue.

Video 2: Depiction of z-directional ortho slices used to reconstruct lipid droplets in 2-year murine brown adipose tissue.

Video 3: Arc shot of 3D reconstructed lipid droplet overlaid on ortho slice in 3-month murine brown adipose tissue.

Video 4: Arc shot of 3D reconstructed lipid droplet overlaid on ortho slice in 2-year murine brown adipose tissue.

Video 5: Depiction of z-directional ortho slices used to reconstruct lipid droplet-mitochondrial interactions in 3-month murine brown adipose tissue.

Video 6: Depiction of z-directional ortho slices used to reconstruct lipid droplet-mitochondrial interactions in 2-year murine brown adipose tissue.

Video 7: Arc shot of 3D reconstructed lipid droplet-mitochondrial interactions overlaid on ortho slice in 3-month murine brown adipose tissue.

Video 8: Arc shot of 3D reconstructed lipid droplet-mitochondrial interactions overlaid on ortho slice in 2-year murine brown adipose tissue.

Graphical Abstract

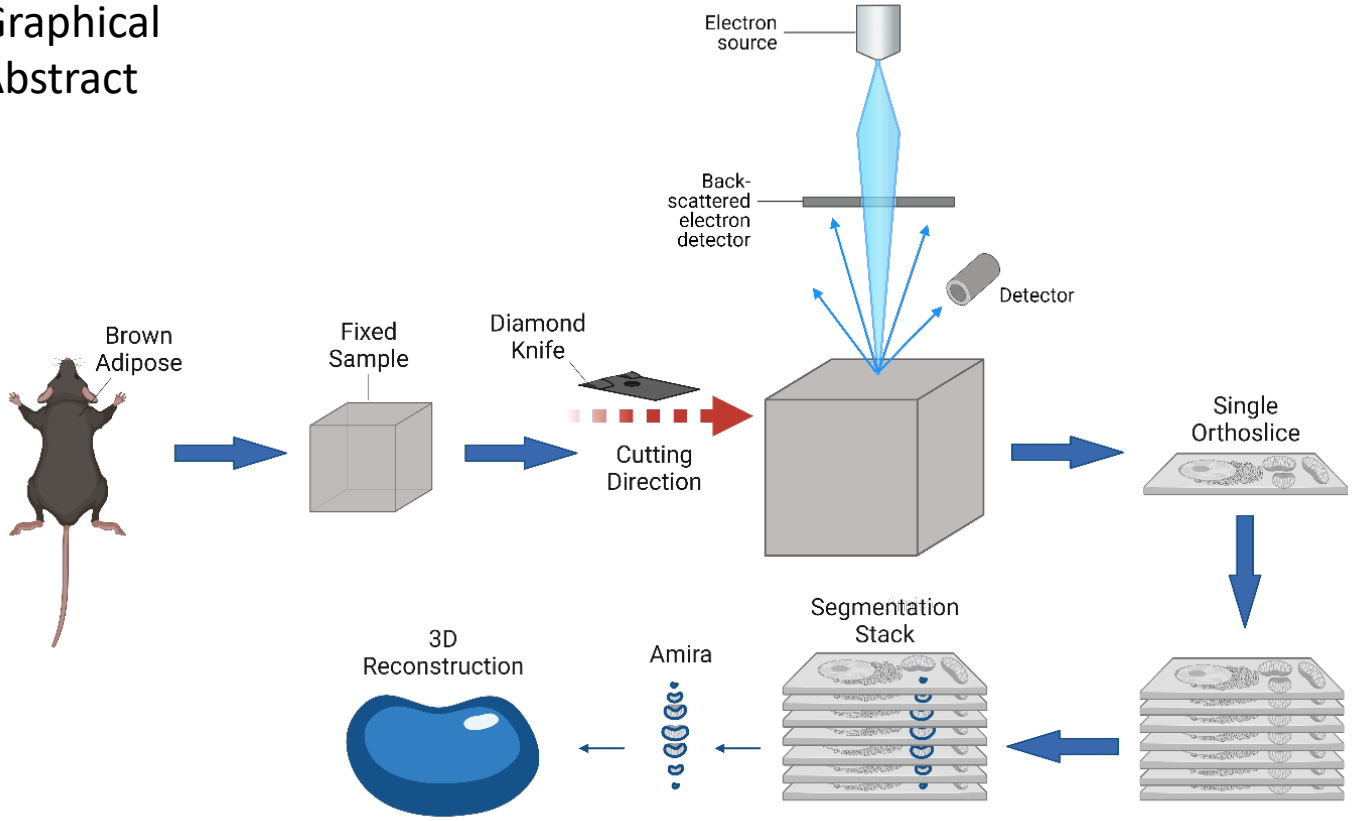

Figure 1

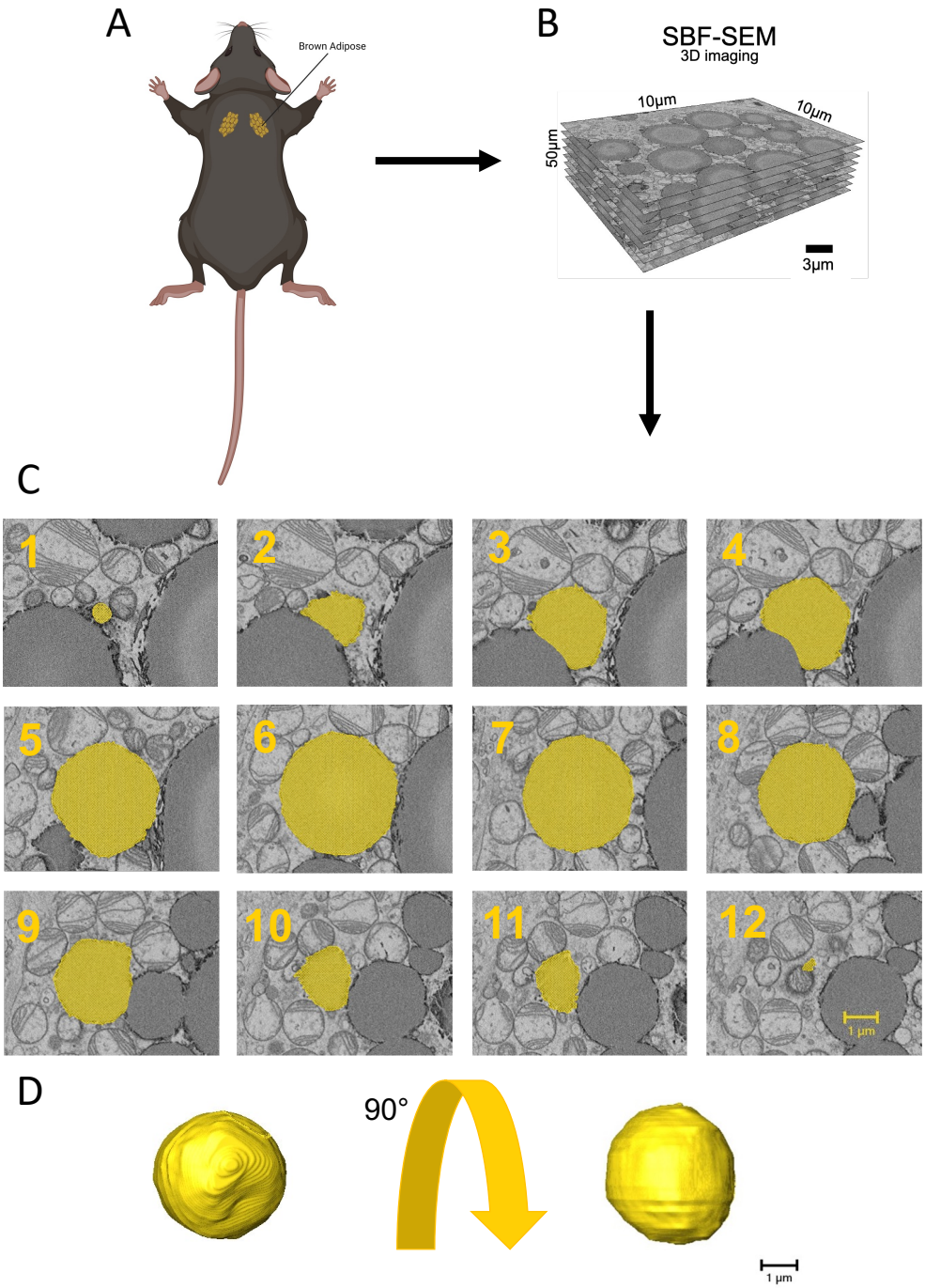
A
Brown Adipose
B
SBF-SEM
3D imaging
10µm
10µm
50µm
3µm
C
1
2
3
4
5
6
7
8
9
10
11
12
1 µm
D
90°
1 µm

Figure 2

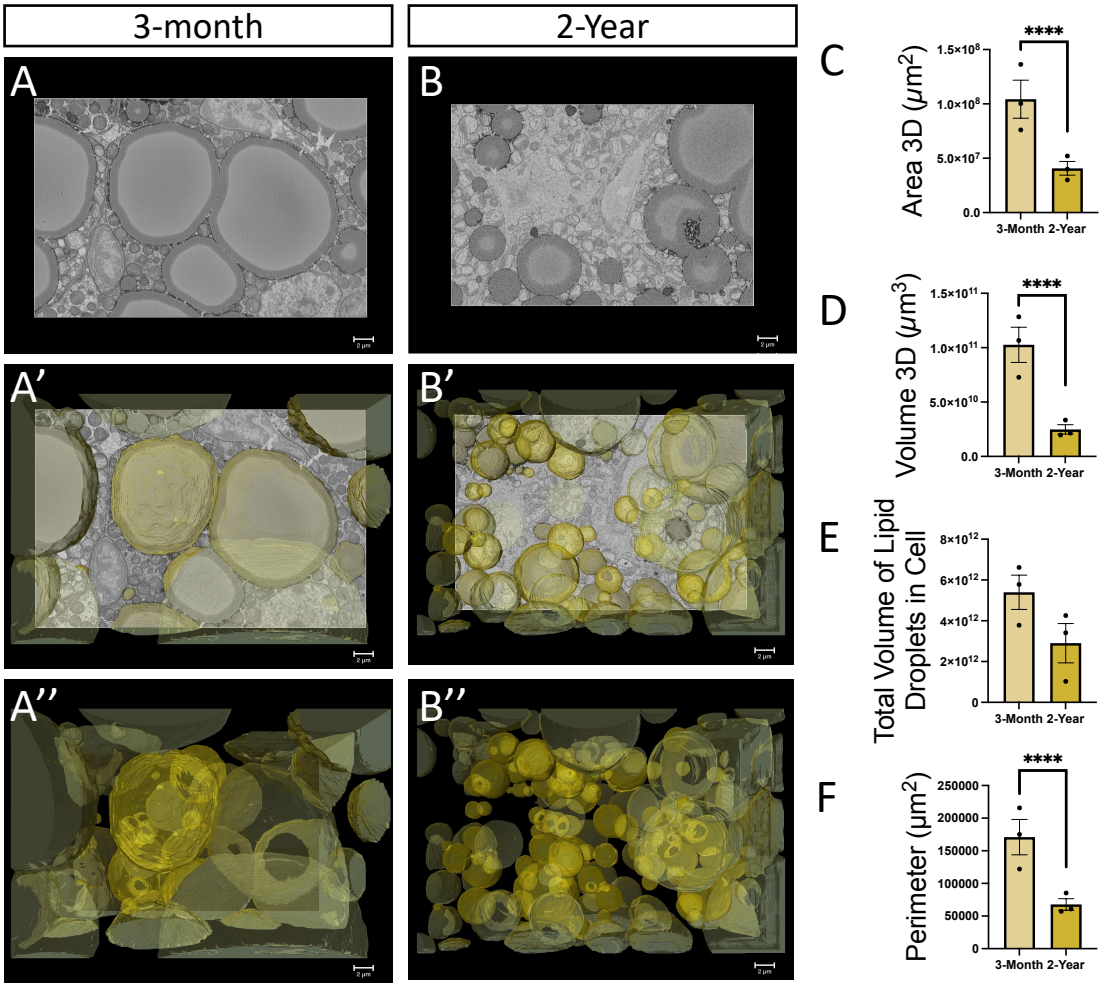
3-month
2-Year
A
B
A'
B'
A''
B''
C
Area 3D (μm²)
1.5×10⁸
1.0×10⁸
5.0×10⁷
0.0
****
3-Month 2-Year
D
Volume 3D (μm³)
1.5×10¹¹
1.0×10¹¹
5.0×10¹⁰
0.0
****
3-Month 2-Year
E
Total Volume of Lipid Droplets in Cell
8×10¹²
6×10¹²
4×10¹²
2×10¹²
0
3-Month 2-Year
F
Perimeter (μm²)
250000
200000
150000
100000
50000
0
****
3-Month 2-Year

Figure 3

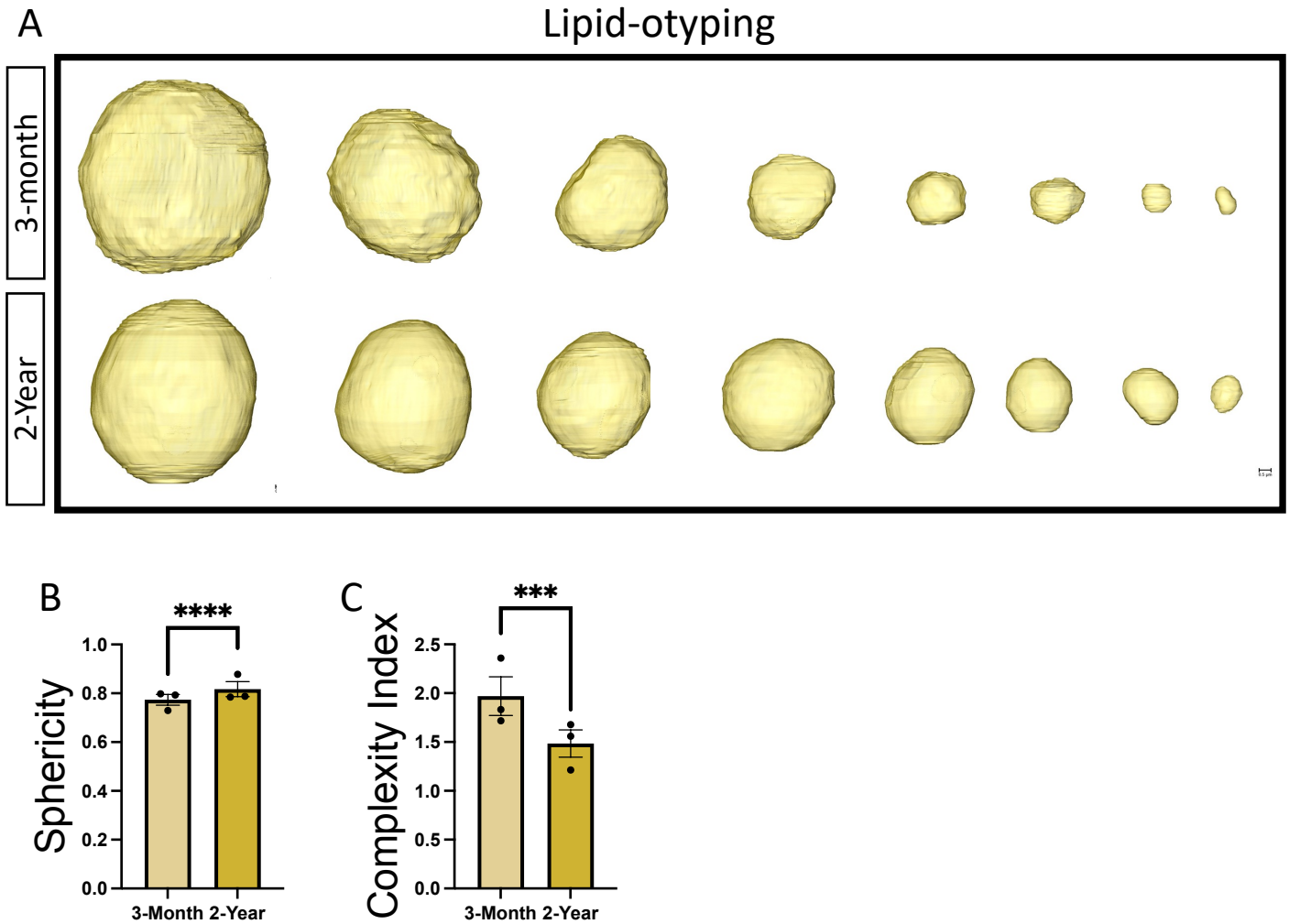
A
Lipid-otyping
3-month
2-Year
B
****
Sphericity
1.0
0.8
0.6
0.4
0.2
0.0
3-Month 2-Year
C
***
Complexity Index
2.5
2.0
1.5
1.0
0.5
0.0
3-Month 2-Year

Figure 4

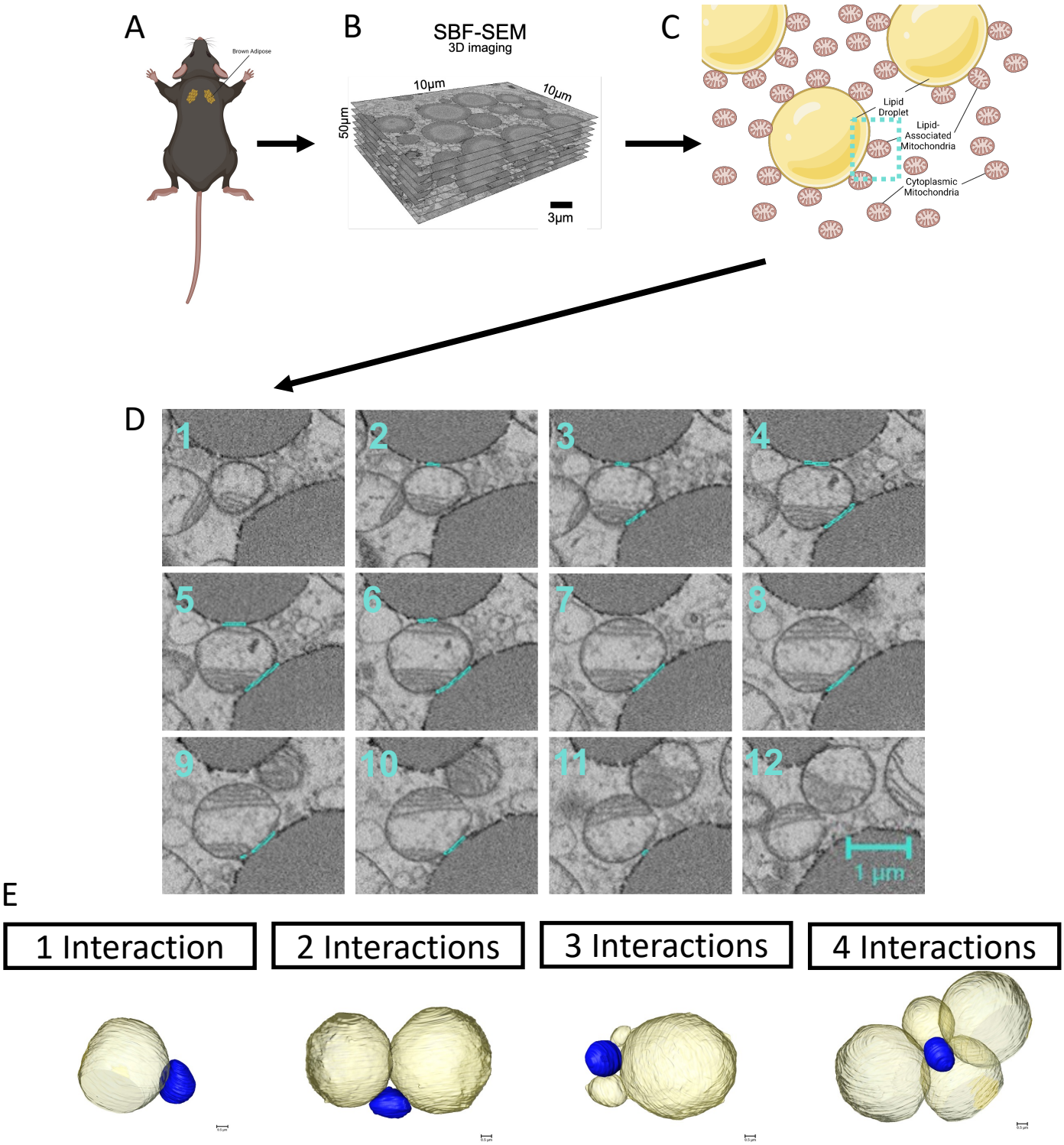
A
Brown Adipose
B
SBF-SEM
3D imaging
10µm
10µm
50µm
3µm
C
Lipid Droplet
Lipid-Associated Mitochondria
Cytoplasmic Mitochondria
D
1
2
3
4
5
6
7
8
9
10
11
12
1 µm
E
1 Interaction
2 Interactions
3 Interactions
4 Interactions

Figure 5

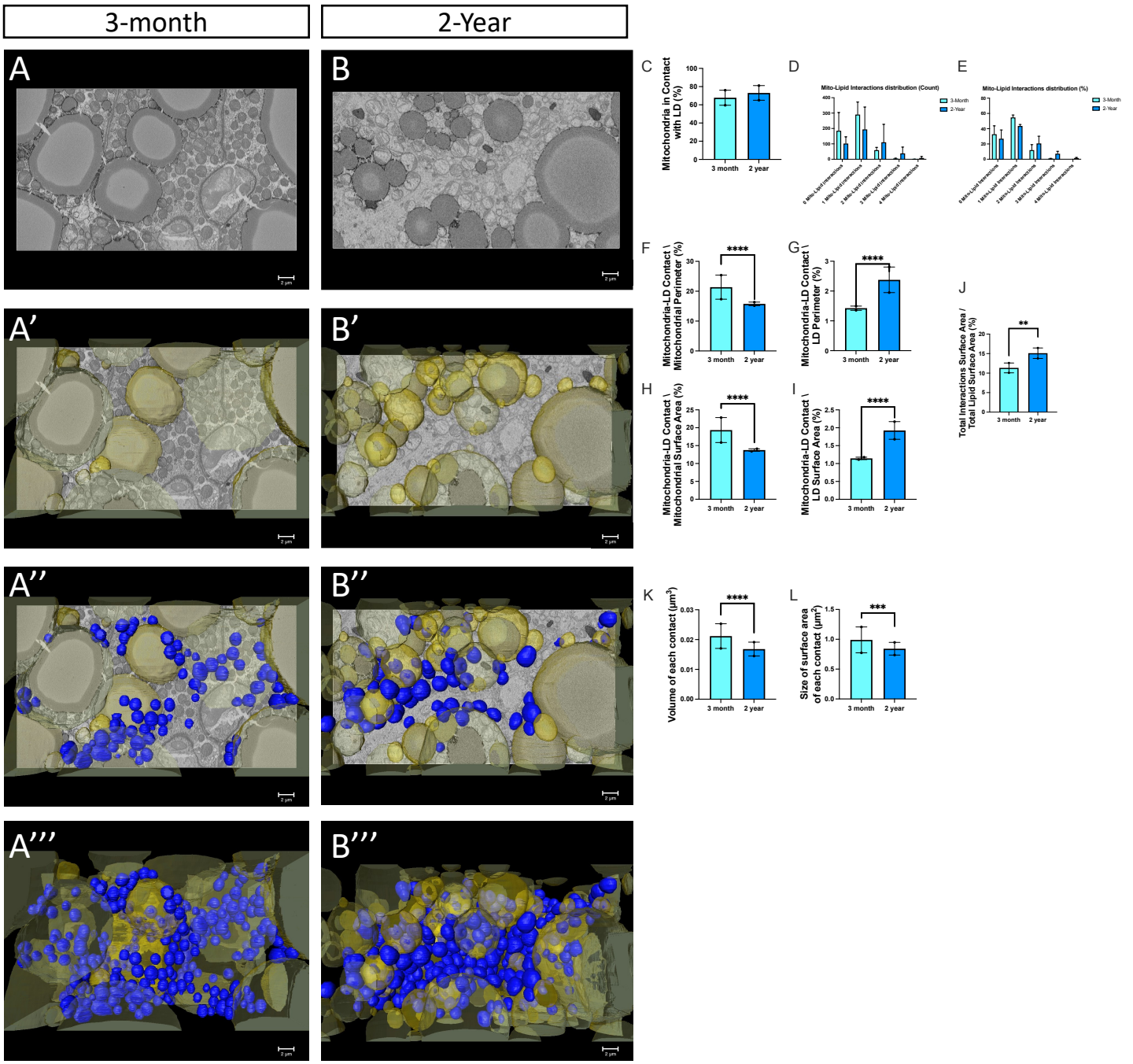
3-month
2-Year
A
B
A'
B'
A''
B''
A'''
B'''
C
Mitochondria in Contact with LD (%)
3 month
2 year
D
Mito-Lipid Interactions distribution (Count)
3-Month
2-Year
E
Mito-Lipid Interactions distribution (%)
F
Mitochondria-LD Contact \ Mitochondrial Perimeter (%)
****
G
Mitochondria-LD Contact \ LD Perimeter (%)
J
Total Interactions Surface Area / Total Lipid Surface Area (%)
**
H
Mitochondria-LD Contact \ Mitochondrial Surface Area (%)
I
Mitochondria-LD Contact \ LD Surface Area (%)
K
Volume of each contact (µm³)
L
Size of surface area of each contact (µm²)
***

Figure 6

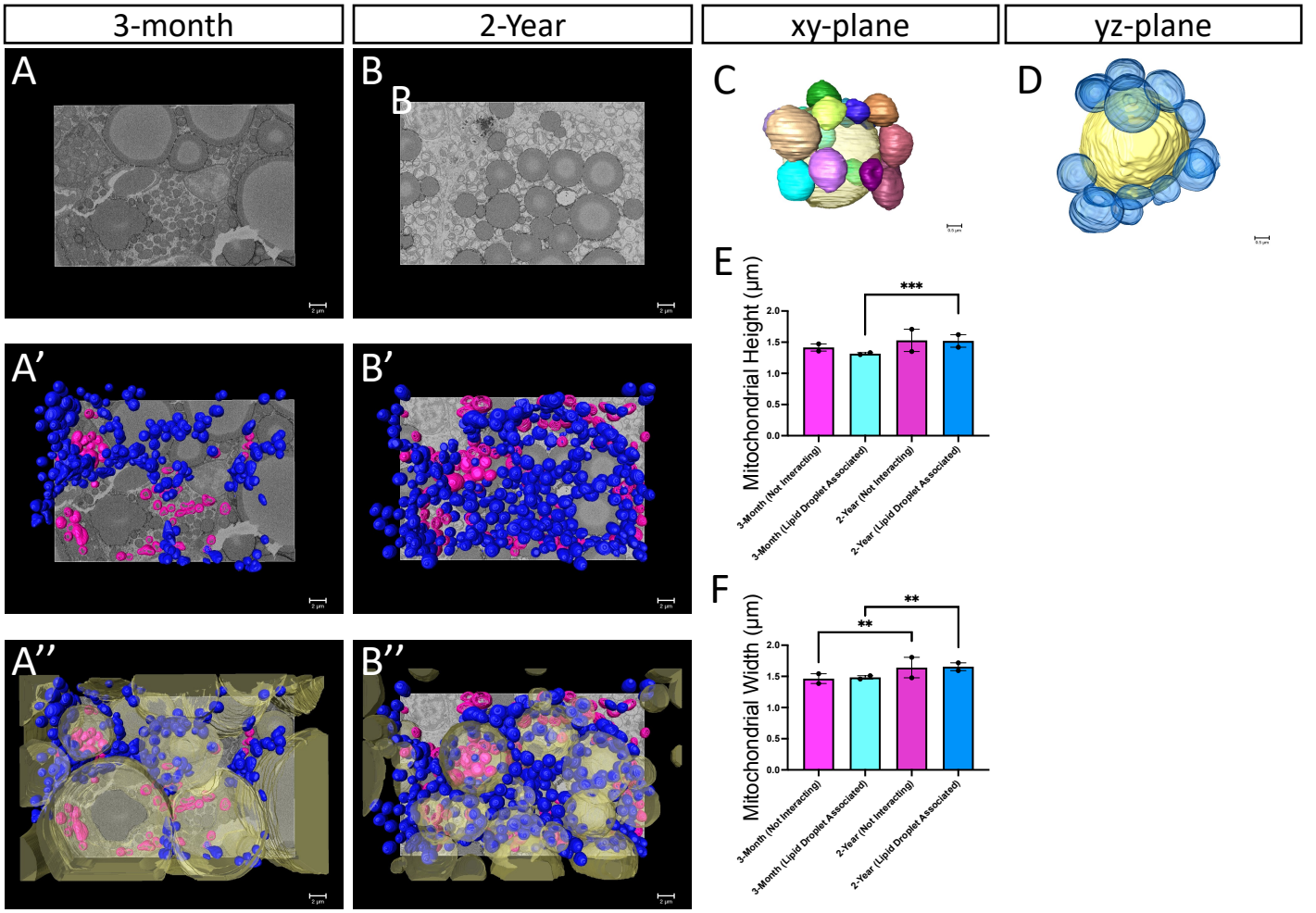
3-month
2-Year
xy-plane
yz-plane
A
B
B
C
D
A'
B'
A''
B''
E
Mitochondrial Height (µm)
***
2.0
1.5
1.0
0.5
0.0
3-Month (Not Interacting)
3-Month (Lipid Droplet Associated)
2-Year (Not Interacting)
2-Year (Lipid Droplet Associated)
F
Mitochondrial Width (µm)
**
**
2.0
1.5
1.0
0.5
0.0
3-Month (Not Interacting)
3-Month (Lipid Droplet Associated)
2-Year (Not Interacting)
2-Year (Lipid Droplet Associated)